Nuclear Magnetic Resonance Assignments and Global Fold of a CheY-Binding Domain in CheA, the Chemotaxis-Specific Kinase of *Escherichia coli*[†]

Megan M. McEvoy,[‡] Hongjun Zhou,[‡] Amy F. Roth,[§] David F. Lowry,[‡] Tom B. Morrison,[‖] Lewis E. Kay,[⊥] and Frederick W. Dahlquist*,[‡]

Institute of Molecular Biology, University of Oregon, Eugene, Oregon 97403, Biology Department, University of Utah, Salt Lake City, Utah 84112, and Protein Engineering Network Centres of Excellence and Departments of Medical Genetics, Biochemistry, and Chemistry, University of Toronto, Toronto, Ontario, Canada, M5S 1A8

Received May 25, 1995; Revised Manuscript Received August 17, 1995[⊛]

ABSTRACT: CheA is the histidine autokinase in the *Escherichia coli* chemotaxis signal transduction pathway responsible for coupling of signals received by transmembrane receptors to the response regulators CheY and CheB. Here NMR spectroscopy is used to study a 14 kDa fragment of CheA, residues 124–257, that binds the response regulator CheY. Backbone atom resonance assignments were obtained by analysis of 3D HNCACB, 3D CBCA(CO)NH, and HNCO spectra, whereas side-chain assignments were obtained primarily by analysis of 3D H(CCO)NH, 3D C(CO)NH, 3D HCCH-TOCSY, and 3D ^{1}H,^{15}N TOCSY-HSMQC spectra. NOE cross peak patterns and intensities as well as torsion angle restraints were used to determine the secondary structure, and a low-resolution structure was calculated by hybrid distance-geometry simulated annealing methods. The CheA124–257 fragment consists of four antiparallel β strands and two helices, arranged in an "open-faced β-sandwich" motif, as well as two unstructured ends that correspond to domain linkers in the full-length protein. The ^{15}N–^{1}H correlation spectrum of ^{15}N-labeled CheA124–257 bound to unlabeled CheY shows specific localized changes that may correspond to a CheY-binding face on CheA.

The chemotaxis signal transduction system in *Escherichia coli* allows response to changes in extracellular ligands by biasing movement toward chemical attractants and away from repellents (see Bourret et al. (1991), Stock et al. (1991), and Alex and Simon (1994) for reviews]. Binding of extracellular ligands to periplasmic domains of dimeric membrane-bound receptors causes allosteric changes in the receptors which are sensed by the cytoplasmic components of the signal transduction system (Milburn et al., 1991). On the cytoplasmic side of the membrane-bound receptors is a dimer of the histidine autokinase CheA and two copies of the coupling protein CheW (Gegner & Dahlquist, 1991; McNally & Matsumura 1991; Gegner et al., 1992). The autophosphorylation rate of CheA changes in response to ligand occupancy of the membrane-bound receptors (Borkovich et al., 1989; Borkovich & Simon, 1990; Ninfa et al., 1991; Wolfe et al., 1994). After autophosphorylation of CheA, the phosphate is transferred to the downstream targets: the response regulator CheY and the methylesterase CheB (Hess et al., 1988a; Wylie et al., 1988). Phosphorylated CheY is thought to interact with components of the flagellar motor to cause a change in directional bias of the

flagellum, thereby altering the swimming behavior of the bacterium (Bourret et al., 1990). Phosphorylated CheB increases its methylesterase activity toward the receptors, which subsequently decreases their ability to stimulate CheA autophosphorylation, thus adapting the chemotactic response to the continuing presence of ligand (Borkovich et al., 1992). The chemotaxis signaling system is a member of the "two-component" family of signal transduction pathways, defined by the presence of an autophosphorylating histidine kinase and a conserved response regulator domain which is the target of phosphorylation.

The histidine autokinase CheA is central to the chemotaxis signal transduction system of *E. coli*. Genetic and biochemical evidence indicates that CheA contains an elaborate domain structure. Full-length CheA consists of 654 amino acids organized into five functional domains responsible for phosphotransfer, substrate binding, ATP-binding and catalysis, CheW coupling, and receptor coupling (Figure 1). The site of autophosphorylation, histidine 48, is located within the P1 domain, residues 1–134 (Hess et al., 1988b; Swanson et al., 1993). The residues of CheA primarily responsible for interaction with the response regulator CheY are in the P2 domain of CheA, approximately within residues 160–233 (Swanson et al., 1993; Morrison & Parkinson, 1994). The catalytic activity of the CheA kinase is located within the central domain of CheA, residues 260–537 (Swanson et al., 1993). The domains that may be responsible for CheW coupling and receptor coupling are located at the carboxy terminus (Liu, 1992; Bourret et al., 1993; T. B. Morrison, unpublished observations).

The P2 domain of CheA has been defined by a number of biochemical and genetic techniques. On the basis of

* Author to whom correspondence should be addressed.
‡ University of Oregon.
§ Present address: Department of Surgery, Wayne State University School of Medicine, Detroit, MI 48201.
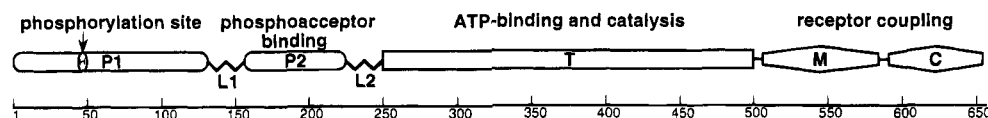‖ University of Utah.
⊥ University of Toronto.

FIGURE 1: Schematic representation of the domain organization of CheA. The N-terminal phosphotransfer domain, P1, contains a histidine at position 48 which is the site of autophosphorylation. The P2 domain contains the residues primarily responsible for interaction with the response regulator CheY. The central kinase domain, T, contains the ATP binding and catalysis functions. The M and C domains may couple CheA to the receptor and CheW.

protease sensitivity experiments and sequence alignment with CheA from *Salmonella typhimurium*, residues 124–257 of CheA from *E. coli* are thought to contain two regions corresponding to domain linkers in the intact protein, L1 and L2, as well as a compactly folded domain of approximately 65 amino acids, P2 (Parkinson & Kofoid, 1992; Swanson et al., 1993; Morrison & Parkinson, 1994). Because protein fragments containing residues 160–233 bind to CheY with an affinity similar to that of full-length CheA (Swanson et al., 1993, 1995; J. Li, R. V. Swanson, M. I. Simon, and R. M. Weis, unpublished observations), the P2 domain is likely to contain the primary determinants responsible for binding CheY. Overexpression of residues 124–257 *in vivo* inhibits chemotactic response (Morrison & Parkinson, 1994), presumably because CheY is being sequestered and signal transfer to the flagellar motor is prevented. This domain may confer the specificity required in the chemotaxis signal transduction system which may be necessary to insulate the many two-component signal transduction pathways within the cell from each other.

Here we report the results obtained from multidimensional NMR[1] experiments performed on the CheA fragment containing the CheY-binding domain of CheA, residues 124–257. CheA124–257 has been found to contain a structured segment of 68 amino acids, residues 160–227, as well as two unstructured regions at either end of the fragment that correspond to the domain linkers L1 and L2, in agreement with the prediction from sequence comparison and proteolytic experiments. [15]N and ^{13}C/^{15}N uniformly labeled proteins were used to acquire NMR data leading to the backbone and side chain resonance assignments. NOE and coupling constant data were used to determine the secondary structure elements present in the fragment, and hybrid distance-geometry simulated annealing methods using the program X-PLOR (Brünger, 1992) were used to determine the overall topology. Spectra were obtained of ^{15}N uniformly labeled CheA124–257 bound to unlabeled CheY and specific resonance shifts in CheA124–257 were observed, identifying a region of CheA124–257 likely to interact with the phosphoacceptor, CheY. This region corresponds to residues in the loop after the first helix and residues in and around the second helix.

EXPERIMENTAL PROCEDURES

Sample Preparation. CheA124–257 was expressed from the pTM22 plasmid (Morrison & Parkinson, 1994) using the *E. coli* strain K38. This construct encodes residues 124–257 of CheA as well as five additional residues (Ile, Lys,

Leu, Gly, and Thr) at the C-terminal end which are a result of the cloning procedure. Isotopic labeling was achieved by expression of pTM22 grown at 37 °C in minimal media (Sambrook et al., 1989) containing ([15]NH$_4$)$_2$SO$_4$ (Isotec, Inc.) as the sole nitrogen source for ^{15}N uniformly labeled protein samples or ([15]NH$_4$)$_2$SO$_4$ (1 g/L) and [^{13}C]glucose (Isotec, Inc.) (2 g/L) as the sole nitrogen and carbon sources for ^{15}N/^{13}C uniformly labeled protein samples. At OD$_{600}$ = 0.5, cells were induced with 1 mM isopropyl β-D-thiogalactopyrano-side (IPTG), harvested after 3.5 h, and lysed by sonication. Cell debris was pelleted by centrifugation at 35000g. CheA124–257 was precipitated from the supernatant by addition of 50% ammonium sulfate and pelleted by centrifugation at 17400g. Protein was resuspended in 10 mM MOPS, 0.5 mM EDTA, and 25 mM KCl, pH 7.2 (MEK25), and 1 mM phenylmethanesulfonyl fluoride and dialyzed against MEK25 before application to an Affi-Gel Blue (Bio-Rad Laboratories, Richmond, CA) column at 4 °C equilibrated with MEK25. Fractions were assayed by SDS–PAGE, and those containing CheA124–257 were pooled and applied to a DE52 (Whatman Laboratory Division, Maidstone, England) anion exchange column at 4 °C equilibrated with MEK25 and eluted using a linear gradient from 25 mM KCl to 425 mM KCl in 10 mM MOPS/1 mM EDTA at pH 7.2. Fractions were assayed by SDS–PAGE, and those containing CheA124–257 were pooled and dialyzed against MEK25 and loaded on a Q Sepharose (Pharmacia, Uppsala, Sweden) column equilibrated with MEK25 at 4 °C. CheA124–257 was eluted from the column using a linear gradient from 25 mM KCl to 625 mM KCl in 10 mM MOPS/1 mM EDTA at pH 7.2. Fractions were assayed by SDS–PAGE, and CheA124–257-containing fractions were combined and precipitated with 50% ammonium sulfate. Precipitate was pelleted by centrifugation at 17400g and resuspended in 50 mM sodium phosphate at pH 6.5 and dialyzed into the final NMR buffer. Protein was concentrated using Centriprep-10 and Centricon-3 concentrators (Amicon). Final protein concentrations were estimated by bicinchoninic acid (BCA) assay (Bollag & Edelstein, 1991), because the protein contains no tryptophan or tyrosine residues. NMR samples contained 2–6 mM protein in 50 mM sodium phosphate at pH 6.5, 0.02% sodium azide in 90% H$_2$O/10% D$_2$O. For the deuterium exchange experiments, a spin column containing Sephadex G25 in 50 mM sodium phosphate in 99.9% D$_2$O was used to exchange the solvent of a sample containing 2 mM protein from H$_2$O to D$_2$O immediately before acquisition of the spectra.

NMR Spectroscopy. Triple-resonance spectra were recorded on a single sample of 4 mM ^{13}C/^{15}N uniformly labeled CheA124–257 in 50 mM sodium phosphate, pH 6.5, at 30 °C on a Varian UNITY 500 MHz spectrometer equipped with a pulsed field gradient unit and an actively shielded 5 mm [1]H–[15]N–[13]C triple-resonance probe. All of the triple-resonance experiments were recorded using a strategy to minimize saturation and dephasing of water magnetization

---

[1] Abbreviations: DQF-COSY, double-quantum-filtered correlation spectroscopy; HSMQC, heteronuclear single-multiple-quantum correlation; HSQC, heteronuclear single-quantum correlation; NMR, nuclear magnetic resonance; NOE, nuclear Overhauser effect; NOESY, nuclear Overhauser effect spectroscopy; rms, root mean square; TOCSY, total correlation spectroscopy; 2D, two dimensional; 3D, three dimensional.

(Grzesiek & Bax, 1993; Stonehouse et al., 1994; Kay et al., 1994).

The sensitivity-enhanced HNCACB (Wittekind & Mueller, 1993; Muhandiram & Kay, 1994) spectrum was acquired as a $38 \times 36 \times 512$ complex matrix using 16 scans per increment. Acquisition times in t_1 ($^{13}C_{\alpha/\beta}$), t_2 (^{15}N), and t_3 (^1H_N) were 4.9, 21.8, and 64.0 ms, respectively. The sensitivity-enhanced CBCA(CO)NH (Grzesiek & Bax, 1992; Muhandiram & Kay, 1994) spectrum was acquired as a $50 \times 32 \times 512$ complex matrix using eight scans per increment. Acquisition times were 6.5 ms in t_1 ($^{13}C_{\alpha/\beta}$), 19.4 ms in t_2 (^{15}N), and 64.0 ms in t_3 (^1H_N). The carrier frequencies for the HNCACB were centered at 43.0 (F_1), 119.0 (F_2), and 4.73 ppm (F_3), and spectral widths were 7649.6, 1650.0, and 8000.0 Hz in F_1, F_2, and F_3, respectively. Identical carrier frequencies and spectral widths were employed for the CBCA(CO)NH with the exception of the carbon carrier which was switched from 43.0 to 58.0 ppm during the course of the experiment as described in Muhandiram and Kay (1994).

The H(CCO)NH and C(CO)NH (Grzesiek et al., 1993) spectra were acquired as $64 \times 32 \times 512$ and $50 \times 32 \times 512$ complex matrices respectively using 16 scans per increment. Acquisition times for the H(CCO)NH were 25.6 ms in t_1 (^1H_C), 19.4 ms in t_2 (^{15}N), and 64.0 ms in t_3 (^1H_N) and for the C(CO)NH were 6.5 ms t_1 (^{13}C), 19.4 ms in t_2 (^{15}N), and 64.0 ms in t_3 (^1H_N). Carrier frequencies for the H(CCO)NH were centered at 4.73, 119.0, and 4.73 ppm in F_1, F_2, and F_3, respectively, and the corresponding spectral widths were 2500.0 Hz in F_1, 1650.0 Hz in F_2, and 8000.0 Hz in F_3. The spectral widths for the C(CO)NH were 7649.6 (F_1), 1650.0 (F_2) and 8000.0 Hz (F_3) with the carrier frequencies centered at 43.0 and 58.0 ppm (Muhandiram & Kay, 1994) in F_1, 119.0 ppm in F_2, and 4.73 ppm in F_3.

The sensitivity-enhanced 3D HNCO (Kay et al., 1990, 1994) spectrum was acquired as a $64 \times 32 \times 512$ complex matrix using four scans per increment. Acquisition times in t_1 ($^{13}C'$), t_2 (^{15}N), and t_3 (^1H_N) were 42.8, 19.4, and 64.0 ms, respectively, with carrier frequencies centered at 177.0, 119.0, and 4.73 ppm in F_1, F_2, and F_3, respectively. Spectral widths were 1495.8, 1650.0, and 8000.0 Hz in F_1, F_2, and F_3, respectively.

The 3D HCCH-TOCSY spectrum in H_2O (Bax et al., 1990; Kay et al., 1993) was acquired as a $128 \times 32 \times 512$ complex matrix with acquisition times of 36.6 ms in t_1 (^1H), 10.7 ms in t_2 (^{13}C), and 64.0 ms in t_3 (^1H). The carrier frequencies were centered at 4.73 ppm in F_1 and F_3 and at 43.0 ppm in F_2. The spectral widths were 3499.9, 3000.0, and 8000.0 Hz in F_1, F_2, and F_3, respectively.

The $^{15}N-^1H$ HSQC correlation spectrum (Bodenhausen & Ruben, 1980; Kay et al., 1992) was acquired as a 128×512 complex matrix with acquisition times of 64 ms in both t_1 and t_2. The spectral widths were 2000.0 Hz in F_1 and 8000.0 Hz in F_2.

Triple-resonance data were processed using the nmrPipe/nmrDraw software developed by Frank Delaglio, NIH (Delaglio, 1993), and analyzed using the program PIPP (Garrett et al., 1991). Typically, data were processed in the acquisition and indirect dimensions with shifted sine-bell squared apodization. All triple-resonance three-dimensional data were zero-filled in F_1 and F_3, and mirror image linear prediction was used in F_2 to result in a final matrix sizes of $128 \times 128 \times 512$ real points, with the exception of the

HCCH-TOCSY where mirror image linear prediction was not used.

The 3D ^1H, ^{15}N NOESY-HSMQC, 3D ^1H, ^{15}N TOCSY-HSMQC, J-modulated [^{15}N, ^1H]COSY, 2D NOESY, 2D DQF-COSY, and HSMQC spectra of the CheA124−257/CheY complex were performed on a General Electric Omega 500 MHz spectrometer equipped with a Nalorac 5 mm triple-resonance probe. Water suppression was achieved by presaturation. All spectra were aquired at 30 °C. The 3D ^1H, ^{15}N NOESY-HSMQC, 3D ^1H, ^{15}N TOCSY-HSMQC, and J-modulated [^{15}N, ^1H]COSY were acquired on a single 4 mM ^{15}N uniformly labeled CheA124−257 sample. Data acquired on the General Electric Omega 500 MHz spectrometer were processed using FELIX software (Hare Research and BioSym Technologies, San Diego, CA).

3D, $^1H,^{15}N$ NOESY-HSMQC experiments, which are a variation of the 3D NOESY-HMQC (Marion et al., 1989a; Zuiderweg & Fesik, 1989) wherein an HSMQC pulse sequence is used to generate $^1H-^{15}N$ coherence, were recorded using 100 and 150 ms mixing times. Each 3D $^1H,^{15}N$ NOESY-HSMQC spectrum was acquired as a matrix of 256 (real) $\times$ 64 (real) $\times$ 1024 (complex) points using 16 scans per increment. The acquisition times in t_1 (^1H), t_2 (^{15}N), and t_3 (^1H_N) were 38.4, 31.5, and 153.6 ms, respectively, with spectral widths of 6666.6 Hz in F_1, 1016.25 Hz in F_2, and 6666.6 Hz in F_3. Quadrature detection in t_1 and t_2 was achieved using TPPI phase incrementation (Marion & Wüthrich, 1983). The carrier frequencies were centered at 4.73 ppm for F_1 and F_3 and at 119.0 ppm for F_2. The 3D $^1H,^{15}N$ TOCSY-HSMQC (Cavanagh et al., 1989; Marion et al., 1989b) spectrum was acquired with parameters identical to those used in the $^1H,^{15}N$ NOESY-HSMQC spectra, with a mixing time of 70 ms using an MLEV-17 pulse train (Bax & Davis, 1985). Quadrature detection in t_1 and t_2 for the $^1H,^{15}N$ TOCSY-HSMQC was achieved using the States method (States et al., 1982).

A series of 10 J-modulated [$^{15}N,^1H$]COSY (Billeter et al., 1992) experiments were acquired to estimate $^3J_{NH\alpha}$ coupling constants. Each 2D experiment was acquired as a 128 (real) $\times$ 1024 (complex) matrix using 64 scans per increment. The acquisition times used were 61.4 ms in t_1 (^{15}N) and 153.6 ms in t_2 (^1H_N) with spectral widths of 1041.6 Hz in F_1 and 6666.6 Hz in F_2. Quadrature detection was achieved using the States−TPPI method (Marion et al., 1989c). Delay times (τ_2) of 9.2, 20.0, 30.0, 50.0, 56.0, 63.0, 71.0, 83.0, 100.0, and 125.0 ms were used in successive experiments. Each experiment was processed identically with shifted sine bell apodization and zero-filled to 1024 and 512 points in the proton and nitrogen dimension, respectively. Measured volumes were plotted as function of the delay time and fit by a curve using nonlinear least-squares methods as described by Billeter et al. (1992).

Hydrogen exchange was performed by passing 0.5 mL of 2 mM ^{15}N-labeled CheA124−257 through a 5 mL Sephadex G25 spin column equilibrated with 50 mM sodium phosphate at pH 6.5 in 99.9% D_2O and immediately placing the sample in an NMR tube. The time elapsed from application of the sample to the D_2O-containing spin column to the start of the acquisition of the HSMQC spectrum was approximately 10 min. The HSMQC spectrum was acquired as a 256 (real) $\times$ 1024 (complex) spectrum with four scans per increment. The acquisition times in t_1 (^{15}N) and t_2 (^1H) were 122.8 and 153.6 ms, respectively, with spectral widths of 1041.7 Hz in F_1 and 6666.6 Hz in F_2. Quadrature detection was

achieved using the States method (States et al., 1982). The total time to acquire the spectrum was 16 min. The carrier frequencies were centered at 119.0 ppm in the F_1 dimension and 4.73 ppm in the F_2 dimension.

The 2D NOESY (Macura & Ernst, 1980; Kumar et al., 1980) and 2D DQF-COSY (Shaka & Freeman, 1983; Rance et al., 1984) spectra were acquired using the same 2 mM ^{15}N-labeled CheA124−257 sample that was used for the hydrogen−deuterium exchange experiments. The 2D NOESY and the 2D DQF-COSY were acquired as 512 (real) × 1024 (complex) matrices, with acquisition times of 38.4 ms in t_1 and 153.6 ms in t_2. Spectral widths were 6666.6 Hz in F_2 and 6666.6 Hz in F_1 for both spectra. Quadrature detection was achieved using the TPPI method (Marion et al., 1983). The carrier frequencies were centered at 4.73 ppm in F_1 and 4.73 ppm in F_2.

To examine the CheY-binding effects on the CheA124−257 fragment, an ∼0.7 mM ^{15}N-labeled CheA124−257 sample in 50 mM sodium phosphate, pH 6.5, 8 mM MgCl$_2$, and 0.02% sodium azide was titrated with unlabeled CheY in the same buffer, and HSMQC (Zuiderweg, 1990) spectra were taken after each addition. CheY protein was prepared as described in Lowry et al. (1994). The spectra were acquired at CheA124−257/CheY ratios of approximately 2.6:1, 1.4:1, 1:1, and 1:2 as 256 (real) × 1024 (complex) matrices using 128 scans per increment. The acquisition times in t_1 (^{15}N) and t_2 (^1H_N) were 79.3 and 153.6 ms, respectively, for all spectra in the titration series. The spectral widths used were 1612.9 Hz in F_1 and 6666.6 Hz in F_2. The carrier frequencies were centered at 119 ppm in F_1 and 4.73 ppm in F_2.

Structure Calculations. Hybrid distance geometry−simulated annealing calculations (Nilges et al., 1988) were used to determine the global fold of the protein using the program X-PLOR (Brünger, 1992). The protocol involves calculating an initial set of structures containing a subset of the atoms (N, Cα, Hα, Cβ, Cγ, C′) for each residue by projection from n-dimensional distance space into Cartesian coordinate space. After calculation of these starting structures, the coordinates of the rest of the atoms were added, followed by refinement using dynamical simulated annealing. During simulated annealing, the target function that is minimized is made up of quadratic harmonic terms arising from covalent geometry requirements, van der Waals repulsion terms, and experimental restraints for distance and torsion angles. The NOE volumes from the ^{15}N, ^{1}H NOESY-HSMQC, and 2D NOESY in D$_2$O solution were estimated and classified as strong, 1.8−3.0 Å, medium, 1.8−4.0 Å, or weak, 1.8−5.0 Å. Structures were calculated using 257 intraresidue, 266 sequential ($|i − j| = 1$), 108 medium-range ($1 < |i − j| ≤ 5$), and 73 long-range ($|i − j| > 5$) NOEs from residues 159−227. Also included were 54 distance restraints (19 hydrogen bonds) for the atoms that participate in hydrogen bonds in the β-sheet and α-helices as judged by the amides present after the first spectrum (26 min) of the hydrogen-deuterium exchange experiments. Hydrogen bonds were defined as N−O bond distances of 2.5−3.5 Å and H−O bond distances of 1.5−2.5 Å. The linker regions of the fragment, residues 124−158 and 228−257, were not included in the structure calculations since their disorder resulted in very few NOEs. The ϕ dihedral angles were measured from the J-modulated [^{15}N,^{1}H]COSY experiments and restrained to be −57° ± 25° for the helical regions with the exception of residues D207 and V211 whose $^3J_{HN\alpha}$ are

not strictly in the range of classical helical residues. The ϕ dihedral angles for the residues in the β-strands were restrained to be −139 ± 25°, with the exceptions of the residues at the end of the strands, and the residues in β-strand 2 which have irregular structure. No ψ dihedral angle restraints were used. Sixty initial structures were calculated. After the preliminary structure calculation, the 51 lowest energy structures were subjected to further rounds of refinement. Thirty-six of these structures exhibited the same overall folding topology. Structures were visualized using the program RasMol v2.5 (Sayle, 1994), MOLSCRIPT (Kraulis, 1991), or O v5.9 (Jones et al., 1991). The average rms deviation of the backbones atoms (N, Cα, C′) of selected structures was calculated using X-PLOR.

RESULTS

Our approach to the structure determination of the CheA124−257 fragment was to make use of scalar connectivities to assign each backbone and side-chain resonance in the CheA fragment. Using the assignments, the ^{1}H,^{15}N NOESY-HSMQC spectra were analyzed to obtain secondary structure information. Further analysis of the NOESY spectra provided long-range NOEs, which were sufficient to determine the global fold of the P2 domain of CheA.

Resonance Assignments. The backbone and Cβ assignments of CheA124−257 were obtained by analysis of the HNCACB and CBCA(CO)NH spectra to determine sequentially connected segments (Figure 2a). The HNCACB experiment links the intraresidue NH, ^{15}N, Cα, and Cβ shifts and provides connectivities between the NH and ^{15}N shifts and the Cα and Cβ shifts of the previous residue, while the CBCA(CO)NH links NH and ^{15}N shifts with the Cα and Cβ shifts of the preceding residue. By analysis of Cα and Cβ chemical shifts to narrow the range of amino acid possibilities (Wishart et al., 1991), most segments could be unambiguously placed within the protein sequence. The concomitant analysis of the H(CCO)NH and C(CO)NH spectra to further determine amino acid type aided in the placement of short segments of connectivities and confirmed assignments made on the basis of the Cα and Cβ chemical shifts observed in the HNCACB and CBCA(CO)NH spectra. The quality of the spectra was sufficient to obtain H$_N$, N, Cα, and Cβ assignments for 129 out of 131 non-proline residues, with the two residues at the N-terminus unassigned.

The ^{15}N−^{1}H backbone assignments, which provide a "fingerprint" of the protein, are displayed in the HSQC correlation spectrum (Figure 3). The protein fragment contains 139 residues, eight of which are prolines. Although the 2D HSQC spectrum does not contain the expected 131 backbone amide peaks because of the poor dispersion of the amides in the linker region, all but two of the expected number of peaks can be resolved in the HNCACB and CBCA(CO)NH spectra. Of the six glutamine residues in the CheA124−257 fragment, only one is contained within the P2 domain of the protein (residue 220), yet the overlap in the HSQC spectra is still too great to assign more than one of the two δ protons of the glutamine 220 side chain.

Once the backbone proton and nitrogen assignments were made, the HNCO experiment was used to assign the carbonyl carbons for each residue. The carbonyl carbon assignments were obtained for all but 22 residues that either precede a proline or suffer severe chemical shift overlap. Most of the resonances for which the carbonyl carbon assignments could
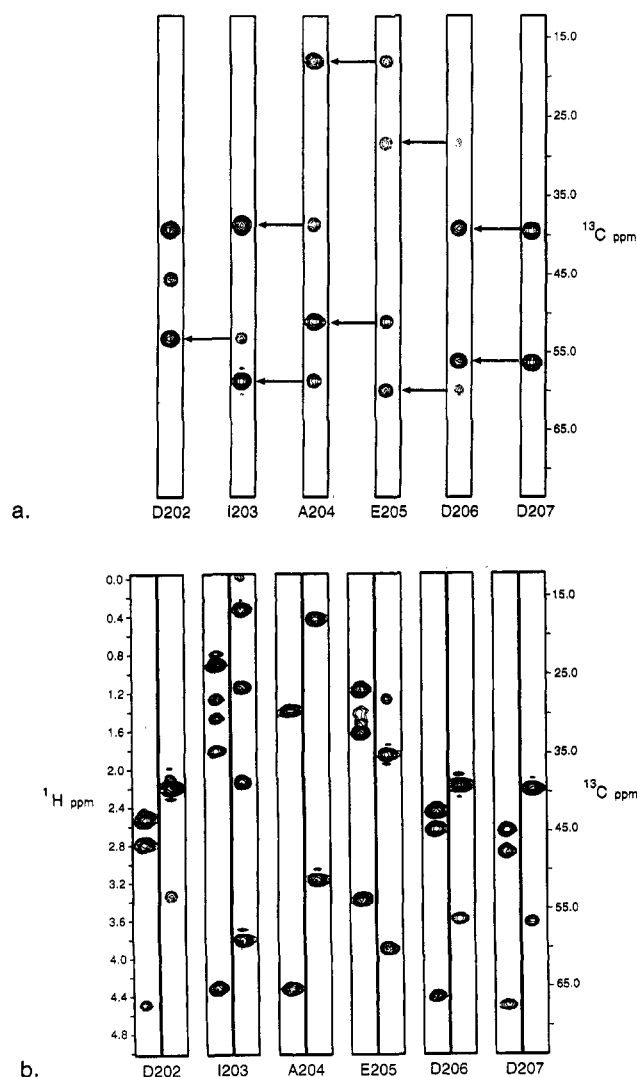
FIGURE 2: (a) Selected regions of the 3D HNCACB spectrum illustrating sequential connectivities for residues 202−207 of CheA124−257. Each ^{1}H−^{13}C strip is plotted at the ^{15}N frequency of the indicated residue. Lines connect the intraresidue correlations with the interresidue correlations. (b) Strips from the H(CCO)NH (left) and C(CO)NH (right) spectra corresponding to residues 202−207 of CheA124−257. In each strip the expected number of protons or carbons can be observed.

not be made were in the linker regions of the protein fragment.

Side-chain assignments were initially made on the basis of analysis of the H(CCO)NH and C(CO)NH spectra, in which side-chain correlations are made to the backbone H_N and N of the following residue (Grzesiek et al., 1993). Overall, the transfer of magnetization out the side chain was very efficient, and most proton and carbon resonances are present even in the long side chain residues (Figure 2b). In many cases, the correlation of side-chain protons to carbons could be made on the basis of the chemical shift values characteristic for particular nuclei at each position in the side chain (Wüthrich, 1986; Wishart et al., 1991). These correlations were verified by examination of the 3D HCCH-TOCSY in H_2O, which worked exceptionally well for the majority of the residues in the fragment. Unfortunately, for much of the linker region, residues 124−159 and 228−257, the overlap of the side chain resonances was too great to obtain these correlations. Therefore, assignments for many of these residues are based only on the H(CCO)NH and C(CO)NH spectra, using knowledge of the chemical shift

values; thus some of the protons of the long-chain residues cannot be correlated unambiguously with side-chain carbons. Aromatic side-chain resonances for the phenylalanine residues F214 and F223 were identified in the 2D DQF-COSY spectrum, and these assignments were supported by observation of intraresidue NOE cross peaks between the corresponding α and β protons from the 2D NOESY in D_2O solution. The side-chain protons for H181 were not observed because of overlap of Hα with residual water. Resonance assignments are available as supporting information.

Secondary Structure Determination. The ^{1}H,^{15}N NOESY-HSMQC spectrum was analyzed for NOEs characteristic of helices or β-strands (Figure 4). In α-helical structures, the amide protons have many short- and medium-range NOE cross peaks that are readily identifiable and indicative of helical structure (Wüthrich, 1986). Two regions, residues 171−180 and 205−212, show large H_{Ni}−H_{Ni+1} cross peaks and also H_{Ni}−H_{Ni+2}, $H_{\alpha i}$−H_{Ni+3}, and $H_{\alpha i}$−H_{Ni+4} cross peaks. These regions also display small (<6 Hz) scalar coupling constants between the amide proton and the α proton, $^3J_{HN\alpha}$, in J-modulated ^{15}N−^{1}H COSY spectra, supporting the classification of these regions as helical. Because the NOE cross peak patterns at the ends of helices are often difficult to distinguish from those NOEs seen in turns, the C-terminal ends of the helices were assigned on the basis of the last residue that is protected from hydrogen exchange. Two residues in the second helix, D207 and V211, have intermediate $^3J_{HN\alpha}$ values (6.3 and 6.6 Hz, respectively) which are not consistent with a classical α-helix geometry (Wüthrich, 1986). This helix may have slight irregularities, yet the other short- and medium-range connectivities are consistent with its classification as an α-helix.

Examination of the ^{1}H,^{15}N NOESY-HSMQC spectra revealed four stretches of strong $H_{\alpha i}$−H_{Ni+1} cross peaks, which suggest β-strands (Figure 4). These regions also contain large $^3J_{HN\alpha}$ values indicating an extended structure as would be expected in β-strands, though the coupling constants of A192 and A197 were not measured because of overlap. Long-range NOE cross peaks (H_α−H_α, H_α−H_N, and H_N−H_N) were observed between neighboring strands; the observed pattern is characteristic of that expected for antiparallel β-strands. The long-range NOE cross peaks specify the arrangement of strands with respect to one another as β2−β3−β1−β4 (Figure 5). For the most part, the connectivities expected for regular antiparallel structures could be seen, with the exception of the second β-strand. This strand is only four residues in length and may contain some irregularities that result in an absence of the expected NOEs between neighboring strands. The α protons of K190 and I198 were not observed because these α protons are at the water resonance and are therefore obscured.

Hydrogen−deuterium exchange was performed in order to probe the accessibility of amides to solvent. Those residues with buried or hydrogen-bonded amide protons are likely to be protected from exchange (Englander & Kallenbach, 1983). The hydrogen exchange patterns in the β-strands (Figure 4) are consistent with the proposed arrangement of β-strands in that the two β-strands (Figure 5) in the middle of the sheet are protected from exchange from both sides, whereas the β-strands on the edge show alternating protections on the sides facing the interior β-strands. Additionally, the hydrogen−deuterium exchange patterns have helped to identify the C-terminal ends of the
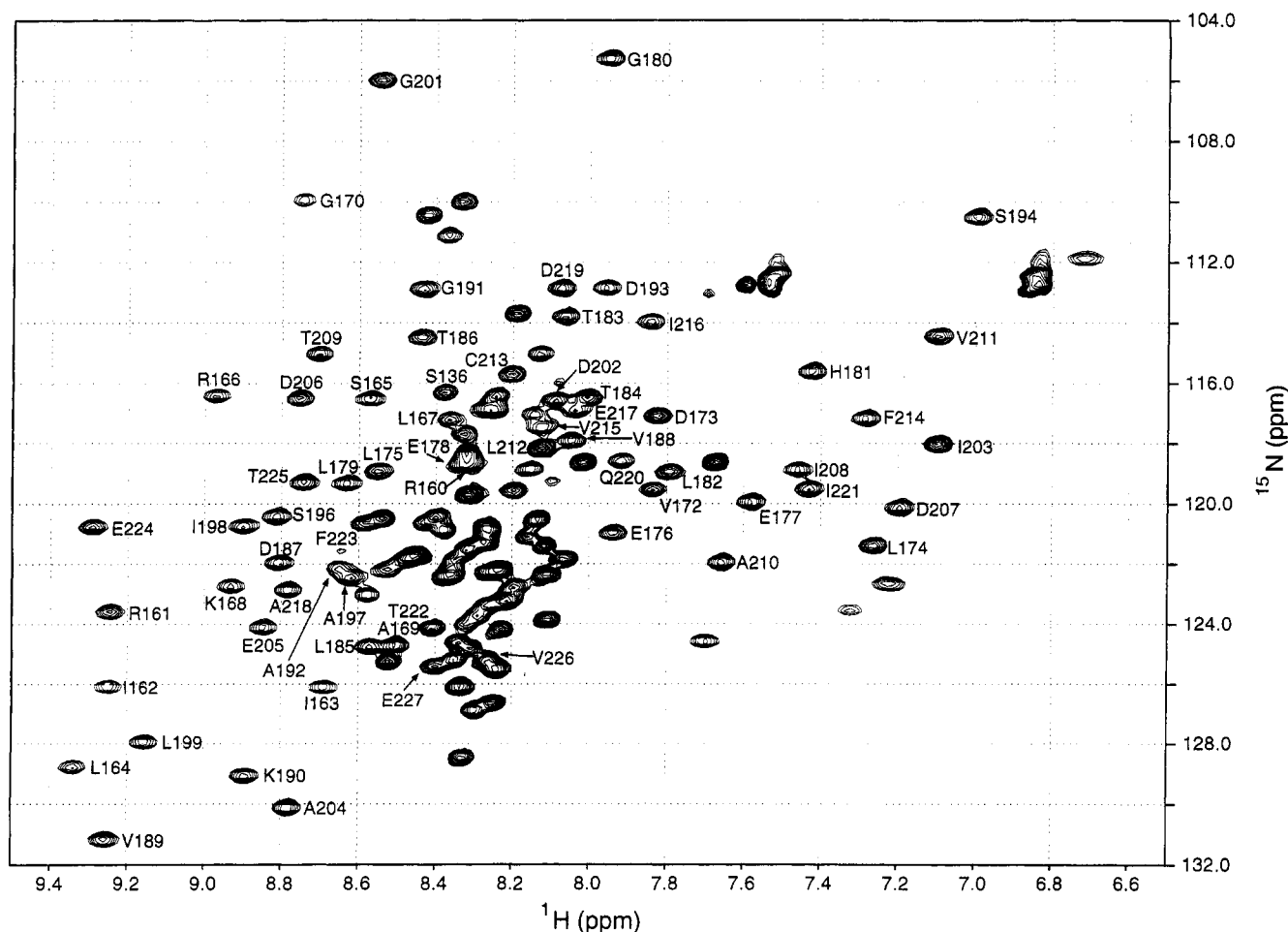
FIGURE 3: $^{15}N-^1H$ correlation spectrum of 4 mM ^{15}N-labeled CheA124−257 in 50 mM sodium phosphate at pH 6.5, 30 °C. Assignments of backbone amide peaks corresponding to residues in the ordered region of the protein are indicated; labels for those peaks that correspond to the disordered region are omitted for clarity.

helices, where the last amide in the helix is protected by hydrogen bonding within the helix.

Residues 124−159 and 228−257, which correspond to the 11 C-terminal residues of domain P1 and to the domain linker regions in CheA, have very few NOE cross peaks in the $^1H,^{15}N$ NOESY-HSMQC. In addition, the low proton chemical shift dispersion for these residues suggests that these regions are unstructured (Figure 3). All the glutamine residues but one are in the linker region, and the lack of chemical shift dispersion for the primary amides of these side chains is evident by their high overlap in the HSQC spectrum. The dynamics data for residues in this region also suggest that these regions are very mobile and disordered (M. M. McEvoy, H. Zhou, and F. W. Dahlquist, unpublished observations).

Determination of the Global Fold of CheA124−257. The $^1H,^{15}N$ NOESY-HSMQC spectra yielded a total of 704 NOE distance restraints within residues 159−227 of the P2 domain of CheA, of which 108 were medium ($1 < |i - j| \leq 5$) and 73 were long range ($|i - j| > 5$). Analysis of the *J*-modulated $^1H-^{15}N$ COSY spectra yielded 39 backbone ϕ dihedral angle restraints, and residues that were classified as being in helices or β-strands were assigned average ϕ dihedral angle restraints for the appropriate secondary structures. Hybrid distance geometry−simulated annealing calculations using the program X-PLOR (Brünger, 1992) were used to determine the overall fold of the P2 domain of CheA. Variations in the accepted structures were seen

predominantly in the helical regions and loops, where there are relatively few long-range NOE distance restraints to position the helices (Figure 6a). The average of nine final low-energy structures were calculated using X-PLOR (Brünger, 1992) and subjected to a cycle of restrained energy minimization to remove any undesireable angles and contacts that may have arisen during the averaging procedure (Figure 6b). The rms deviation about the average structure of the backbone atoms (N, Cα, C′) for the nine structures is 1.76 Å, whereas the rms deviation for all heavy atoms is 2.17 Å.

NMR Spectra of the CheA124−257/CheY Complex. One phosphoacceptor of CheA is the 14 kDa cytosolic response regulator CheY. The portion of CheA that interacts with CheY lies mainly, perhaps exclusively, within residues 124−257 (Swanson et al., 1993; Morrison & Parkinson, 1994). To determine which residues of CheA interact with CheY, NMR spectra of ^{15}N-labeled CheA124−257 were observed in complex with unlabeled CheY. An ^{15}N-labeled sample of CheA124−257 was titrated with unlabeled CheY, and HSMQC spectra were obtained after each addition. Increasing concentrations of CheY caused specific changes in the CheA124−257 spectra (Figure 7). The dissociation constant of the CheA/CheY complex is less than 2 μM (Swanson et al., 1995; J. Li, R. V. Swanson, M. I. Simon, and R. M. Weis, unpublished observations), so CheA124−257 is likely to be >90% bound at the concentrations used in this experiment. On the basis of the movement of the peaks and the line broadening seen at intermediate CheY levels, the
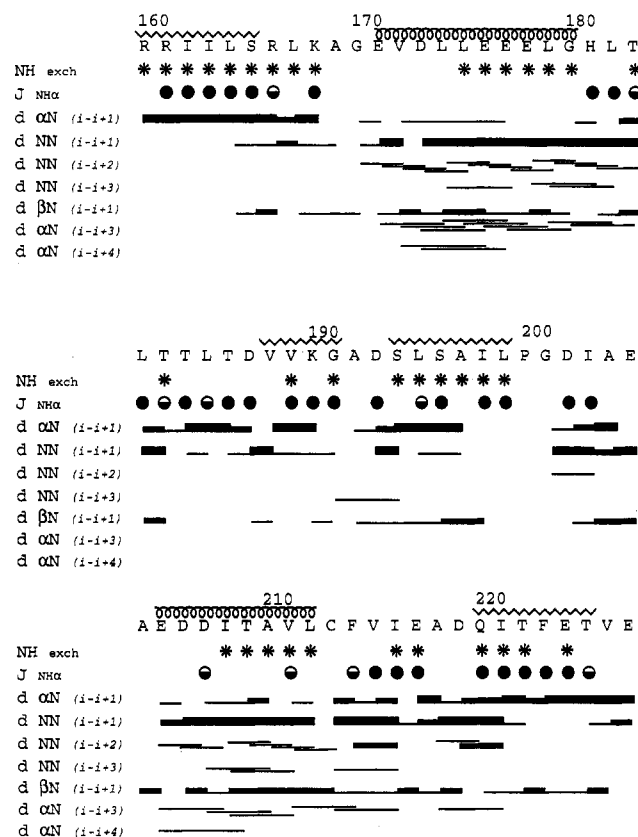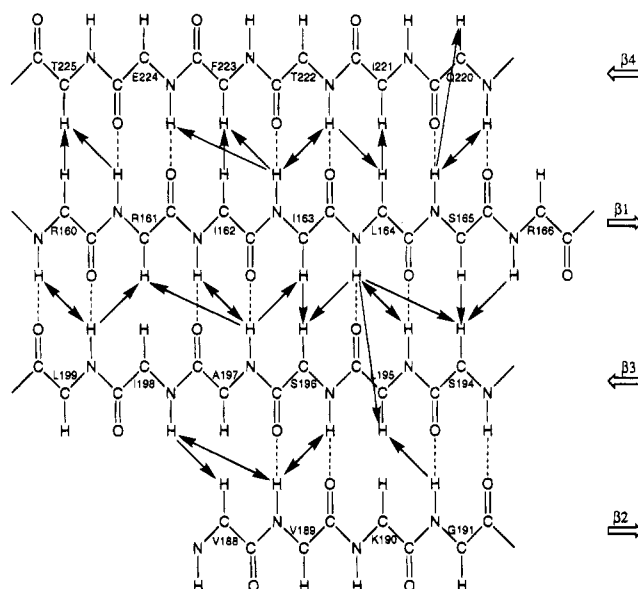
FIGURE 5: Representation of the interstrand NOE contacts observed in the β-sheet region of CheA124−257. NOEs are depicted as arrows, and hydrogen-bonded pairs are depicted by dashed lines.

FIGURE 4: Diagram of the short- and medium-range NOE connectivities observed in residues 160−227 of CheA determined from the 3D ^{1}H,^{15}N NOESY-HMQC and 2D DQF-COSY in 50 mM sodium phosphate at pH 6.5, 30 °C. Residues corresponding to the disordered linker region are omitted, since there are very few NOE cross peaks from these regions. The thickness of the line corresponds to the intensity of each NOE cross peak. The asterisks represent amide protons that are still present after 26 min in D$_2$O solution at pH 6.5, 30 °C. Residues with a $^3J_{HN\alpha}$ coupling constant of greater than 7 Hz are labeled with a filled circle. Residues with intermediate $^3J_{HN\alpha}$ values (6−7 Hz) are labeled with a half-filled circle, and no circles are drawn for the residues with $^3J_{HN\alpha}$ values less than 6 Hz. The secondary structure features are indicated above the sequence of the protein.

CheA124−257/CheY complex appears to be in the intermediate-exchange regime. Peaks could be tracked from one titration point to the next in most cases on the basis of the direction and magnitudes of the changes. The resonances assigned to the peaks in the disordered linker region could not be tracked unambiguously from one spectrum to the next because of overlap, yet these peaks appear qualitatively unchanged even after addition of a 2-fold molar excess of CheY. Most of the significant resonance changes in the spectrum occur in the turn after the first α-helix and in and around the second α-helix (Figure 8). No significant changes in peak position were observed for resonances assigned to the β-sheet, the first α-helix, or the disordered linker regions.

DISCUSSION

From the NOE cross peaks observed in the ^{1}H,^{15}N NOESY-HSMQC, we have been able to determine the secondary structure and the overall fold of the phosphoacceptor-binding domain of CheA, residues 160−227. The domain folds into a compact structure consisting of four strands and two helices, organized as $\beta1-\alpha1-\beta2-\beta3-\alpha2-\beta4$, which forms an "open-faced β-sandwich" (Richardson, 1981), alternately termed as a "split $\alpha\beta$ sandwich" (Orengo

et al., 1994). The low resolution of the current structure does not permit the placement of the helices with great precision, as most of the long-range NOE cross peaks are between the β-strands. The positional disorder of the helices in the final structures is likely due to the paucity of long-range spectroscopic restraints for these helices in our current data set, rather than to mobility or fluctuations of the helices. The lack of NOE cross peaks between the helices is a result of the position of these helices over the outside strands of the β-sheet.

Comparison of the amino acid sequences of the family of kinases in two-component systems shows them to consist of a number of homologous domains (Parkinson & Kofoid, 1992). However, the exact order and number of these domains varies in individual kinases. The fact that the amino and carboxy termini of the P2 domain are in close proximity (Figure 6a,b) may allow this domain to be inserted into an existing polypeptide topology with a little disruption, akin to SH2 or SH3 domains (Musacchio et al., 1992; Waksman et al., 1992).

The topology of this domain of CheA is similar to the topology of a number of other unrelated proteins from both prokaryotes and eukaryotes. Although members of the "split $\alpha\beta$ sandwich" domain superfamily have a common fold, members may share neither sequence nor functional homology (Orengo et al., 1994). Other representatives of this domain superfamily are the histidine-containing phosphocarrier (HPr) (Herzberg et al., 1992; Zongchao et al., 1993; Wittekind et al., 1990; Van Nuland et al., 1994), the activation domain of procarboxypeptidase A (Coll et al., 1991), *E. coli* aspartate transcarbamylase (Gouaux et al., 1990), the RNA-binding domain of the U1 ribonucleoprotein (Nagai et al., 1990), and the L7/L12 ribosomal protein (Leijonmarck & Liljas, 1987). By contrast, the phosphotransfer domain of CheA, residues 1−134, is a member of the "up-down" superfamily (Orengo et al., 1994; Zhou et al., 1995).

The residues at each end of the CheA124−257 fragment are disordered, as evidenced by lack of NOE cross peaks and low chemical shift dispersion. Residues 124−134, which form part of an ordered C-terminal helix of domain
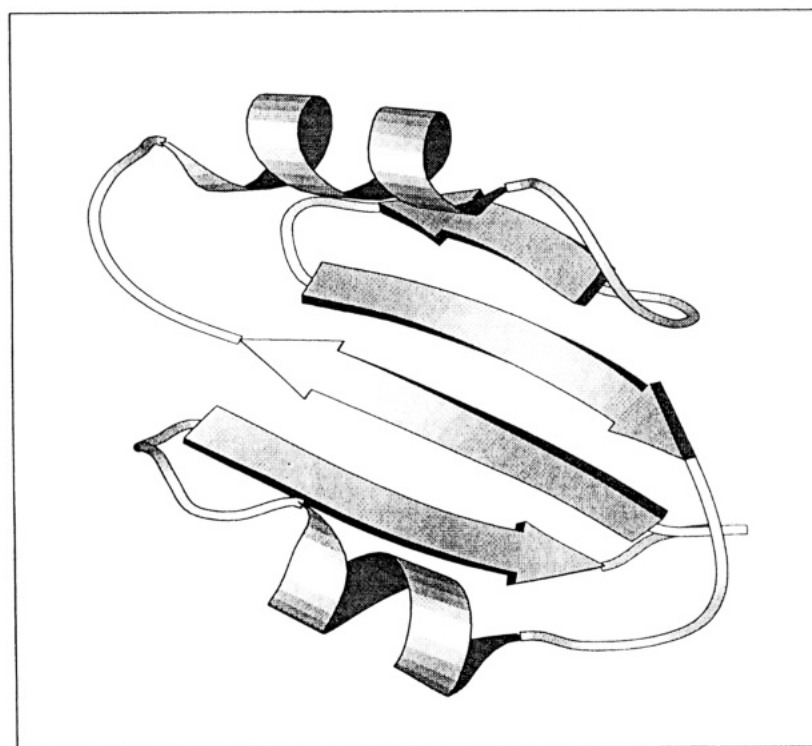
FIGURE 6: (a) Stereoview of the overlay of the α carbon traces of nine final minimized structures of residues 159−227 of CheA. (b) MOLSCRIPT (Kraulis, 1991) ribbon representation of the restrained minimized average of the nine structures depicted in panel a shown in the same orientation.

P1 in the CheA1−134 fragment (Zhou et al., 1995), are disordered in the CheA124−257 fragment. The linker regions, residues 135−159 and 228−257, are readily susceptible to proteolytic cleavage in the full-length protein (Morrison & Parkinson, 1994). The autophosphorylation site of CheA, histidine 48, is located in the N-terminal P1 domain adjacent to the phosphoacceptor-binding P2 domain discussed in this paper. These two domains are connected by a highly charged linker whose flexibility could be important for autophosphorylation and subsequent phosphotransfer

(Parkinson & Kofoid, 1992). NMR studies of a larger fragment of CheA consisting of residues 1−233 indicate that the residues corresponding to the linker between the phosphotransfer and CheY-binding domains is disordered in this construct as well (H. Zhou, M. M. McEvoy, D. F. Lowry, R. V. Swanson, M. I. Simon, and F. W. Dahlquist, unpublished observations). Parkinson and Kofoid (1992) pointed out that communication domains in signaling proteins are often joined by flexible linkers and that these pliable linkers may be important for function. Autophosphorylation
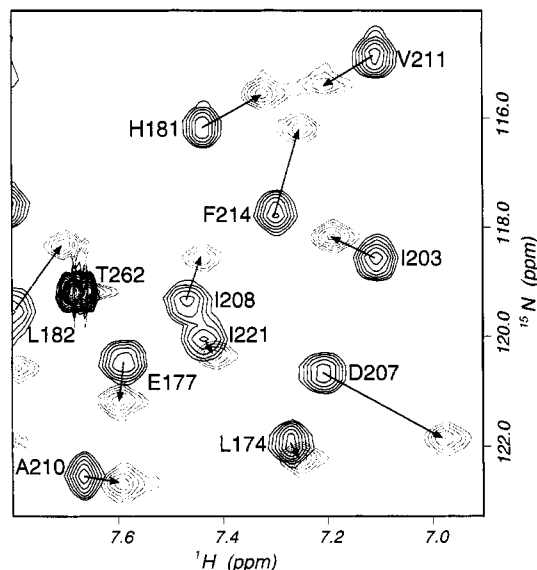
FIGURE 7: Overlay of sections of the $^{15}N-^1H$ correlation spectra of ^{15}N-labeled CheA124−257 free (bold) and bound (light) to CheY in 50 mM sodium phosphate at pH 6.5, 30 °C. These two spectra are the initial and final spectra of the titration of ^{15}N-labeled CheA124−257 with unlabeled CheY; CheY is in approximately 2-fold molar excess to CheA. The arrows show the movement of the peaks.
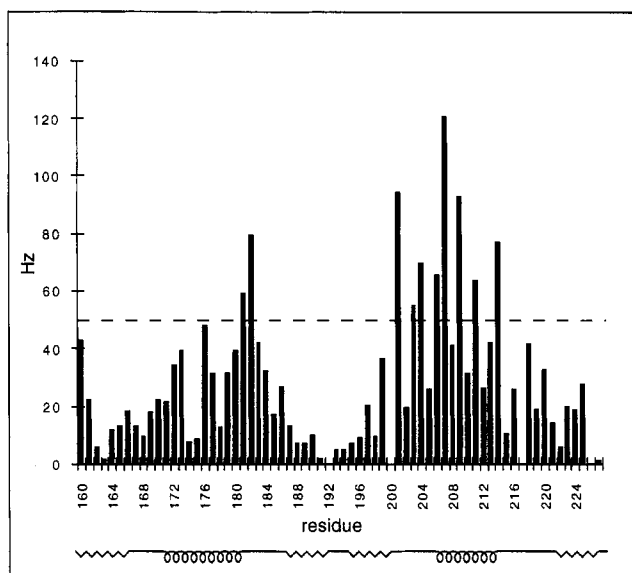

FIGURE 8: Chemical shift changes in the P2 domain (residues 160−227) of CheA124−257 resulting from CheY binding. Shifts were calculated using the formula square root$[(^1H\ Hz)^2 + (^{15}N\ Hz)^2]$. The secondary structure features are displayed at the bottom of the plot.

of histidine 48 requires interaction with the kinase domain, while phosphotransfer requires histidine 48 to come in contact with the phosphoacceptor bound to the P2 domain. Flexible linkers may provide the means of interaction with both the P2 and kinase domain.

The resonances in CheA124−257 that shift upon binding of the phosphoacceptor CheY are primarily located in the loop after the first helix, residues H181 and L182, and in and around the second helix, residues G201, I203, A204, D206, D207, T209, V211, and F214. Although a chemical shift change is not proof of a direct interaction, it is indicative of a structural change in the vicinity. It is likely that at least a subset of the residues whose chemical shifts change upon the addition of CheY are involved in direct interactions. On

the basis of the global fold of the molecule, the helices are on the same side of the β-sheet, though distant from each other. The placement of the helices at the edge of the domain leaves a hydrophobic cleft between them which may have a role in interactions with CheY or the other phosphoacceptor CheB. A binding face on the surface of CheY for CheA1−233 has been identified by NMR (Swanson et al., 1995). The CheA-binding face on CheY is adjacent to the aspartate that is phosphorylated (Asp 57) and does not occlude access by the phosphodonor domain of CheA (residues 1−134).

E. coli has at least 18 two-component regulatory systems that use kinases and response regulators homologous to CheA and CheY for various kinds of sensory signaling in the cell (Swanson & Simon, 1994). The specificity of CheA for CheY may be conferred by the P2 domain, which is absent from other kinases of the two-component family in *E. coli*. The CheY response regulator from *S. typhimurium* is nearly identical to that of *E. coli*; the CheA P2 domains of these organisms are highly homologous as well (Parkinson & Kofoid, 1992). Conversely, these P2 domains have little sequence homology to those in CheA homologs from *Rhizobium meliloti* and *Bacillus subtilis*, whose CheY proteins also differ from their enteric counterparts. Thus the P2 domain may serve to localize or orient CheY to assist in phosphate transfer and may be one means of minimizing cross-talk. With the report of the structure of the P1 domain (Zhou et al., 1995) and this article on the structure of the P2 domain of CheA, we now have the first pieces of structural information for kinases in this class of "two-component" systems. The structural features observed in these domains may prove to be conserved in the modular design of other kinases in this class.

ACKNOWLEDGMENT

SUPPORTING INFORMATION AVAILABLE

Table S-1 showing ^1H, ^{13}C, and ^{15}N NMR assignments for CheA124−257 at 30 °C, in 50 mM sodium phosphate, pH 6.5, and Table S-2 giving NOE distance and dihedral angle restraints (X-PLOR input files) used to determine the overall topology (19 pages). Ordering information is given on any current masthead page.

REFERENCES

Alex, L. A., & Simon, M. I. (1994) *Trends Genet. 10*, 133−138.

Bax, A., & Davis, D. G. (1985) *J. Magn. Reson. 65*, 355−360.

Bax, A., Clore, G. M., & Gronenborn, A. M. (1990) *J. Magn. Reson. 88*, 425−431.

Billeter, M., Neri, D., Otting, G., Qian, Y. Q., & Wüthrich, K. (1992) *J. Biomol. NMR 2*, 257−274.

Bodenhausen, G., & Ruben, D. J. (1980) *Chem. Phys. Lett. 69*, 185−199.

Bollag, D. M., & Edelstein, S. J. (1991) *Protein Methods*, Wiley, New York.

Borkovich, K. A., & Simon, M. I. (1990) *Cell 63*, 1339−1348.

Borkovich, K. A., Kaplan, N., Hess, J. F., & Simon, M. I. (1989) *Proc. Natl. Acad. Sci. U.S.A. 86*, 1208−1212.

Borkovich, K. A., Alex, L. A., & Simon, M. I. (1992) *Proc. Natl. Acad. Sci. U.S.A. 89*, 6756−6760.

Bourret, R. B., Hess, J. F., & Simon, M. I. (1990) *Proc. Natl. Acad. Sci. U.S.A. 87*, 41−45.

Bourret, R. B., Borkovich, K. A., & Simon, M. I. (1991) *Annu. Rev. Biochem. 60*, 401−441.

Bourret, R. B., Davagnino, J., & Simon, M. I. (1993) *J. Bacteriol. 175*, 2097−2101.

Brünger, A. (1992) *X-PLOR Version 3.1: A System for X-ray Crystallography and NMR,* Yale University Press, New Haven, CT.

Cavanagh, J., Chazin, W. J., & Rance, M. (1989) *J. Magn. Reson. 87*, 110−131.

Coll, M., Guasch, A., Aviles, F. X., & Huber, R. (1991) *EMBO J. 10*, 1−9.

Delaglio, F. (1993) NMRPipe System of Software, National Institutes of Health, Bethesda, MD.

Englander, S. W., & Kallenbach, N. R. (1983) *Q. Rev. Biophys. 16*, 521−655.

Garrett, D. S., Powers, R., Gronenborn, A. M., & Clore, G. M. (1991) *J. Magn. Reson. 95*, 214.

Gegner, J. A., & Dahlquist, F. W. (1991) *Proc. Natl. Acad. Sci. U.S.A. 88*, 750−754.

Gegner, J. A., Graham, D. R., Roth, A. F., & Dahlquist, F. W. (1992) *Cell 70*, 975−982.

Gouaux, J. E., Stevens, R. C., & Lipscomb, W. N. (1990) *Biochemistry 29*, 7702−7715.

Grzesiek, S., & Bax, A. (1992) *J. Am. Chem. Soc. 114*, 6291−6293.

Grzesiek, S., & Bax, A. (1993) *J. Am. Chem. Soc. 115*, 12593−12594.

Grzesiek, S., Anglister, J., & Bax, A. (1993) *J. Magn. Reson., Ser. B 101*, 114−119.

Herzberg, O., Reddy, P., Sutrina, S., Saier, M. H., Jr., Reizer, J., & Kapadia, G. (1992) *Proc. Natl. Acad. Sci. U.S.A. 89*, 2499−2503.

Hess, J. F., Oosawa, K., Kaplan, N., & Simon, M. I. (1988a) *Cell 53*, 79−87.

Hess, J. F., Bourret, R. B., & Simon, M. I. (1988b) *Nature 336*, 139−143.

Jones, T. A., Zou, J. Y., Cowan, S. W., & Kjeldgaard, M. (1991) *Acta Crystallogr. A47*, 110−119.

Kay, L. E., Ikura, M., Tschudin, R., & Bax, A. (1990) *J. Magn. Reson. 89*, 496−514.

Kay, L. E., Keifer, P., & Saarinen, T. (1992) *J. Am. Chem. Soc. 114*, 10663−10665.

Kay, L. E., Xu, G. Y., Singer, A., Muhandiram, D. R., & Forman-Kay, J. (1993) *J. Magn. Reson., Ser. B 101*, 333−337.

Kay, L. E., Xu, G. Y., & Yamazaki, T. (1994) *J. Magn. Reson., Ser. A 109*, 129−133.

Kraulis, P. J. (1991) *J. Appl. Crystallogr. 24*, 946−950.

Kumar, A., Wüthrich, K., & Ernst, R. R. (1980) *Biochem. Biophys. Res. Commun. 95*, 1−6.

Leijonmarck, M., & Liljas, A. (1987) *J. Mol. Biol. 195*, 555−580.

Liu, J. D. (1992) Ph.D. Dissertation, University of Utah.

Lowry, D. F., Roth, A. R., Rupert, P. B., Dahlquist, F. W., Moy, F. J., Domaille, P. J., & Matsumura, P. (1994) *J. Biol. Chem. 269*, 26358−26362.

Macura, S., & Ernst, R. R. (1980) *Mol. Phys. 41*, 92−117.

Marion, D., & Wüthrich, K. (1983) *Biochem. Biophys. Res. Commun. 113*, 967−974.

Marion, D., Kay, L. E., Sparks, S. W., Torchia, D. A., & Bax, A. (1989a) *J. Am. Chem. Soc. 111*, 1515−1517.

Marion, D., Driscoll, P. C., Kay, L. E., Wingfield, P. T., Bax, A., Gronenborn, A. M., & Clore, G. M. (1989b) *Biochemistry 28*, 6150−6156.

Marion, D., Ikura, M., Tschudin, R., & Bax, A. (1989c) *J. Magn. Reson. 85*, 393.

McNally, D. F., & Matsumura, P. (1991) *Proc. Natl. Acad. Sci. U.S.A. 88*, 6269−6273.

Milburn, M. V., Privé, G. G., Milligan, D. L., Scott, W. G., Yeh, J., Jancarik, J., Koshland, D. E., & Kim, S.-H. (1991) *Science 254*, 1342−1347.

Morrison, T. B., & Parkinson, J. S. (1994) *Proc. Natl. Acad. Sci. U.S.A. 91*, 5485−5489.

Muhandiram, D. R., & Kay, L. E. (1994) *J. Magn. Reson., Ser. B 103*, 203−216.

Musacchio, A., Noble, M., Pauptit, R., Wierenga, R., & Saraste, M. (1992) *Nature 359*, 851−855.

Nagai, K., Oubridge, C., Jessen, T. H., & Evans, P. R. E. (1990) *Nature 348*, 515−520.

Nilges, M., Clore, G. M., & Gronenborn, A. M. (1988) *FEBS Lett. 229*, 317−324.

Ninfa, E. G., Stock, A., Mowbray, S., & Stock, J. (1991) *J. Biol. Chem. 266*, 9764−9770.

Orengo, C. A., Jones, D. T., & Thornton, J. M. (1994) *Nature 372*, 631−634.

Parkinson, J. S., & Kofoid, E. C. (1992) *Annu. Rev. Genet. 26*, 71−112.

Rance, M., Sørensen, O. W., Bodenhausen, G., Wagner, G., Ernst, R. R., & Wüthrich, K. (1984) *Biochem. Biophys. Res. Commun. 117*, 479.

Richardson, J. S. (1981) *Adv. Protein Chem. 34*, 167−339.

Sambrook, J., Fritsch, E. F., & Maniatis, T. (1989) *Molecular Cloning, A Laboratory Manual,* Cold Spring Harbor Laboratory, Cold Spring Harbor, NY.

Sayle, R. (1994) RasMol v2.5, A Molecular Visualization Program, Biomolecular Structure, Glaxo Research and Development, Greenford, Middlesex, U.K.

Shaka, A. J., & Freeman, R. (1983) *J. Magn. Reson. 51*, 169−173.

States, D. J., Haberkorn, R. A., & Ruben, D. J. (1982) *J. Magn. Reson. 48*, 286−292.

Stock, J. B., Lukat, G. S., & Stock, A. M. (1991) *Annu. Rev. Biophys. Biochem. 20*, 109−136.

Stonehouse, J., Shaw, G. L., Keeler, J., & Laue, E. (1994) *J. Magn. Reson., Ser. A 107*, 178−184.

Swanson, R. V., & Simon, M. I. (1994) *Curr. Biol. 4*, 234−237.

Swanson, R. V., Schuster, S. C., & Simon, M. I. (1993) *Biochemistry 32*, 7623−7629.

Swanson, R. V., Lowry, D. F., Matsumura, P., McEvoy, M. M., Simon, M. I., and Dahlquist, F. W. (1995) *Nature Struct. Biol.* (in press).

Van Nuland, N. A. J., Hangyi, I. W., Van Schaik, R. C., Berendsen, H. J. C., Van Gunsteren, W. F., Scheek, R. M., & Robillard, G. T. (1994) *J. Mol. Biol. 237*, 544−559.

Waksman, G., Kominos, D., Robertson, S. C., Pant, N., Baltimore, D., Birge, R. B., Cowburn, D., Hanafuss, H., Mayer, B. J., Overduin, M., Resh, M. D., Rios, C. B., Silverman, L., & Kuriyan, J. (1992) *Nature 358*, 646−653.

Wishart, D. S., Sykes, B. D., & Richards, F. M. (1991) *J. Mol. Biol. 222*, 311−333.

Wittekind, M., & Mueller, L. (1993) *J. Magn. Reson., Ser. B 101*, 201−205.

Wittekind, M., Reizer, J., & Klevit, R. E. (1990) *Biochemistry 29*, 7191−7200.

Wolfe, A. J., McNamara, B. P., & Stewart, R.C. (1994) *J. Bacteriol. 176*, 4483−4491.

Wüthrich, K. (1986) *NMR of Proteins and Nucleic Acids,* Wiley, New York.

Wylie, D., Stock, A., Wong, C.-Y., & Stock, J. (1988) *Biochem. Biophys. Res. Commun. 151*, 891−896.

Zhou, H., Lowry, D. F., Swanson, R. V., Simon, M. I., & Dahlquist, F. W. (1995) *Biochemistry 34*, 13858−13870.

Zongchao, J., Vandonselaar, M., Quail, J. W., & Delbaere, L. T. J. (1993) *Nature 361*, 94−97.

Zuiderweg, E. R. P. (1990) *J. Magn. Reson. 86*, 346−357.

Zuiderweg, E. R. P., & Fesik, S. W. (1989) *Biochemistry 28*, 2387−2391.